

Selective Molecular Separation by Interfacially Crystallized Covalent Organic Framework Thin Films

Kaushik Dey, Manas Pal, Shebeeb Kunjattu H., kanhu charan Rouy, Anuja Das, Rabibrata Mukherjee, Ulhas K. Kharul, and Rahul Banerjee

J. Am. Chem. Soc., **Just Accepted Manuscript** • DOI: 10.1021/jacs.7b06640 • Publication Date (Web): 06 Sep 2017

Downloaded from <http://pubs.acs.org> on September 6, 2017

Just Accepted

“Just Accepted” manuscripts have been peer-reviewed and accepted for publication. They are posted online prior to technical editing, formatting for publication and author proofing. The American Chemical Society provides “Just Accepted” as a free service to the research community to expedite the dissemination of scientific material as soon as possible after acceptance. “Just Accepted” manuscripts appear in full in PDF format accompanied by an HTML abstract. “Just Accepted” manuscripts have been fully peer reviewed, but should not be considered the official version of record. They are accessible to all readers and citable by the Digital Object Identifier (DOI®). “Just Accepted” is an optional service offered to authors. Therefore, the “Just Accepted” Web site may not include all articles that will be published in the journal. After a manuscript is technically edited and formatted, it will be removed from the “Just Accepted” Web site and published as an ASAP article. Note that technical editing may introduce minor changes to the manuscript text and/or graphics which could affect content, and all legal disclaimers and ethical guidelines that apply to the journal pertain. ACS cannot be held responsible for errors or consequences arising from the use of information contained in these “Just Accepted” manuscripts.

Selective Molecular Separation by Interfacially Crystallized Covalent Organic Framework Thin Films

Kaushik Dey,^{a,b,†} Manas Pal,^{a,‡} Kanhu Charan Rout,^c Shebeeb Kunjattu H.,^c Anuja Das,^d Rabibrata Mukherjee,^d Ulhas K. Kharul,^{b,c} and Rahul Banerjee^{*a,b}

^a Physical/Materials Chemistry Division, CSIR-National Chemical Laboratory, Pune, India.

^b Academy of Scientific and Innovative Research (AcSIR), New Delhi, India.

^c Polymer Science and Engineering Division, CSIR-National Chemical Laboratory, Pune, India.

^d Instability and Soft Patterning Laboratory, Department of Chemical Engineering, Indian Institute of Technology, Kharagpur, India.

ABSTRACT: Exponential interest in the field of covalent organic frameworks (COFs) stems from the direct correlation between their modular design principle and various interesting properties. However, existing synthetic approaches to realize this goal mainly results in insoluble and unprocessable powders, which severely restrict their widespread applicability. Therefore, developing a methodology for easy fabrication of these materials remains an alluring goal and a much desired objective. Herein, we have demonstrated a bottom-up interfacial crystallization strategy to fabricate these microcrystalline powders as large scale thin films under ambient conditions. This unique design principle exploits liquid-liquid interface as a platform, allowing simultaneous control over crystallization and morphology of the framework structure. The thin films are grown without any support in free-standing form and can be transferred on any desirable substrate. The porous (with **Tp-Bpy** showing highest S_{BET} of $1,151 \text{ m}^2\text{g}^{-1}$) and crystalline thin films having high chemical as well as thermal stability, also hold the merit to tune the thickness as low as sub-100 nm. These nanostructured thin COF films demonstrate remarkable solvent permeance and solute rejection performance. A prominent instance is the **Tp-Bpy** thin film, which displays an unprecedented acetonitrile permeance of $339 \text{ Lm}^{-2}\text{h}^{-1}\text{bar}^{-1}$.

INTRODUCTION

Covalent organic frameworks (COFs) represent a new class of periodically extended covalently bound crystalline porous network structures with tunable design features.¹ COFs have fascinated researchers in recent years due to their enormous potential as selective membranes,² catalyst supports,³ gas storage⁴ and energy storage materials⁵. Crystallization of COFs follows a dynamic reversible chemistry,⁶ where organic building blocks are connected through strong covalent bonds in two or three dimensions. However, crystallization of such polymeric frameworks often leads to internal structural defects due to their compositional inhomogeneities, which limits the overall growth of the crystallites into nanometer domains only.⁷ As a result, most of the conventional COF synthetic approaches offer poor control over the material's morphology and thus result in insoluble and unprocessable microcrystalline powders.⁸ Hence, fabricating these insoluble particles for further application presents a formidable challenge. To overcome this issue, several strategies including top-down and bottom-up approaches have been adapted to grow COFs on surfaces.⁹ However, these strategies require a suitable support, as well as expensive techniques, which restrict their comprehensive implementation.^{9a}

Development of a simple and scalable fabrication method to organize individual COF crystallites into a continuous thin film¹⁰ could be a unique solution to realize the full potential of these materials in advanced technologies like membrane separation. Although thin film composite (TFC)^{11a} membranes dominate industrial separation processes due to their superior permeability and excellent solute retentions, these TFC mem-

branes lack tunable and ordered pore structures, as they are commonly fabricated using amorphous polymers.¹¹ Therefore, to achieve the full advantage of the ordered and nano-sized pore channels (1-2 nm), a technique for the preparation of self-standing thin films, which are exclusively derived from COFs, is highly desirable. Nevertheless, bringing such crystalline materials into a self-standing, crack-free, microporous thin film form with high mechanical integrity is a monumental challenge, and if accomplished, will create a breakthrough in many niche separation processes of industrial and environmental significance.

Interfacial synthesis¹² is a well adapted method for the synthesis of polymer thin films like polyamides and polyesters in the bulk scale.^{11a,11d} However, fabricating self-standing thin films of crystalline organic polymers with long-range ordered structures remains to be realized. Keeping this in perspective, we have decided to establish a protocol for synthesizing the crystalline COF thin films with permanent microporosity *via* a room temperature interfacial crystallization approach. By using this approach, we have prepared highly crystalline COF thin films with thickness ranging from ~50 to 200 nm, utilizing liquid-liquid interface as a template under ambient conditions. Since the typical organic Schiff base reaction can lead to the formation of amorphous polymers, the control over the rate of the reaction at the interface is the crucial aspect to triumph over the crystallization problem.¹³ To resolve this issue, we have introduced a salt mediated technique [amine-*p*-toluene sulphonic acid (PTSA) salt], instead of the free amine in the aqueous phase and the aldehyde in the organic phase. The H bonding within the PTSA-amine salt slows down the diffusion

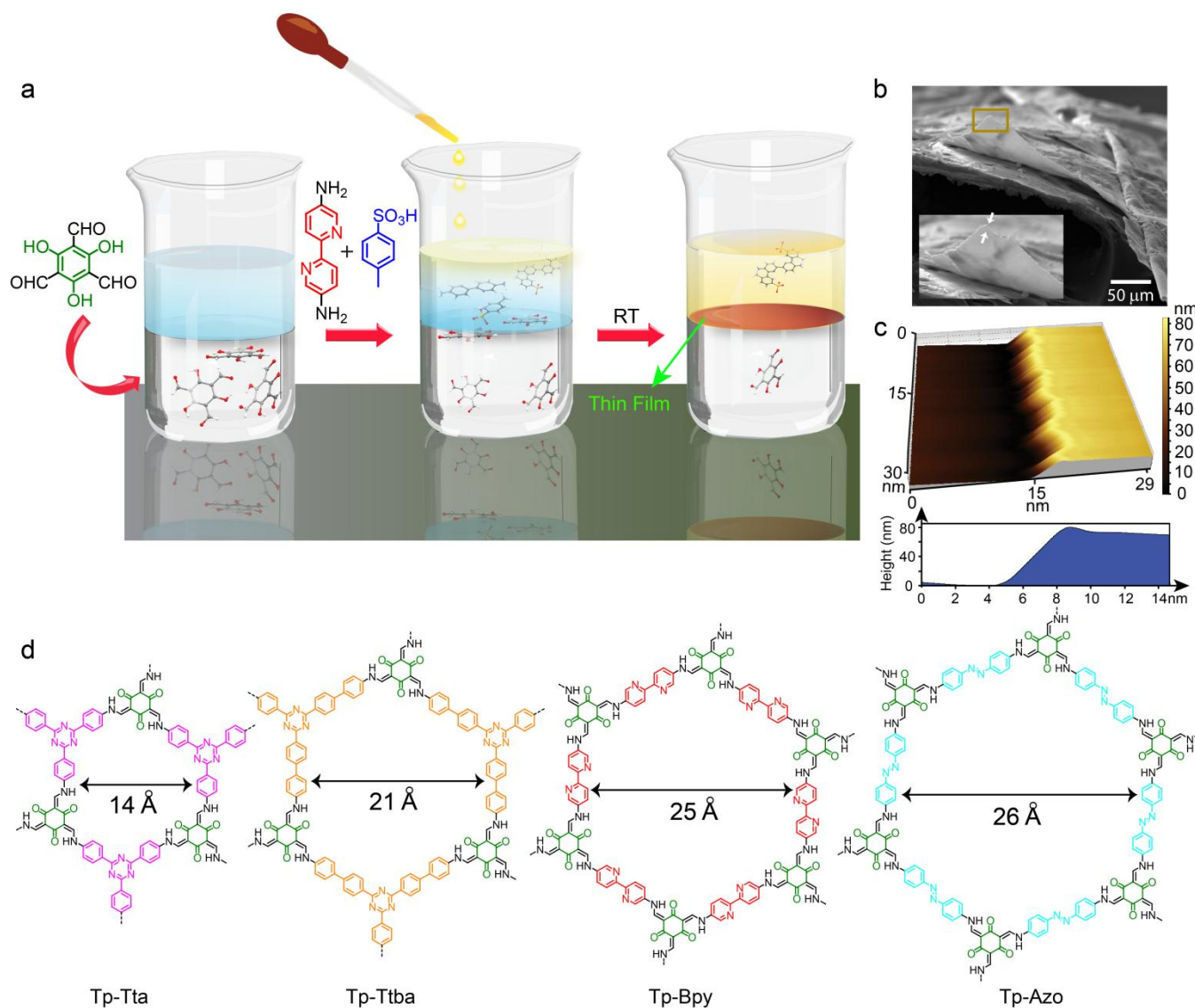


Figure 1. Synthesis scheme of COF thin-films. (a) Schematic representation of the interfacial crystallization process used to synthesize the **Tp-Bpy** thin film. The bottom colorless layer corresponds to aldehyde in dichloromethane solution, the blue layer contains only water as the spacer solution and the top yellow layer is the Bpy amine-PTSA aqueous solution. (b), (c) SEM and AFM image (with corresponding height profile), respectively, of the **Tp-Bpy** thin film synthesized as illustrated in (a). (d) Chemdraw structures of all the COFs used for synthesizing the thin-films *via* interfacial crystallization process.

rate, and this slower diffusion rate of the precursors through the interface drives the reaction towards the thermodynamically controlled crystallization. We have successfully extended this strategy to synthesize four COF thin films having different pore sizes at room temperature. The highly crystalline porous 2D networks are specifically retained at the liquid-liquid interface and are easily transferable to various substrates, including glass surfaces, metallic wires and holey grids, while retaining their physical shape and crystalline structure. Notably, the crystal structures of the self-standing thin-films, as well as their porosities, do not differ from that of their equivalent bulk materials. To the best of our knowledge, this is the first report of an interfacial crystallization of molecular building blocks for creating defect free, self-standing COF thin-films with permanent microporosity. Furthermore, these defect free COF thin films have been successfully used for the selective molecular separations with high solvent permeance. The significance

of thickness control can be easily perceived regarding improved flux values towards water as well as organic solvents.

EXPERIMENTAL SECTION

Synthesis of COF thin films: All four COF thin films **Tp-Bpy**, **Tp-Azo**, **Tp-Ttba** and **Tp-Tta** were synthesized in a glass beaker. First 0.075 mmol of 1,3,5-triformylphloroglucinol (Tp) (15.7 mg) dissolved in 100 mL dichloromethane was poured into the beaker. A spacer layer of 60 mL water was added on top of the aldehyde solution. Finally, 0.112 mmol of diamine [2,2'-bipyridine-5,5'-diamine (Bpy), 20.8 mg; 4,4'-azodianiline (Azo), 23.7 mg]-PTSA (0.224 mmol, 38.5 mg) and 0.075 mmol of triamine [4,4',4''-(1,3,5-triazine-2,4,6-triyl) tris (1,1'-biphenyl) trianiline (Ttba), 43.7 mg; 4,4',4''-(1,3,5-

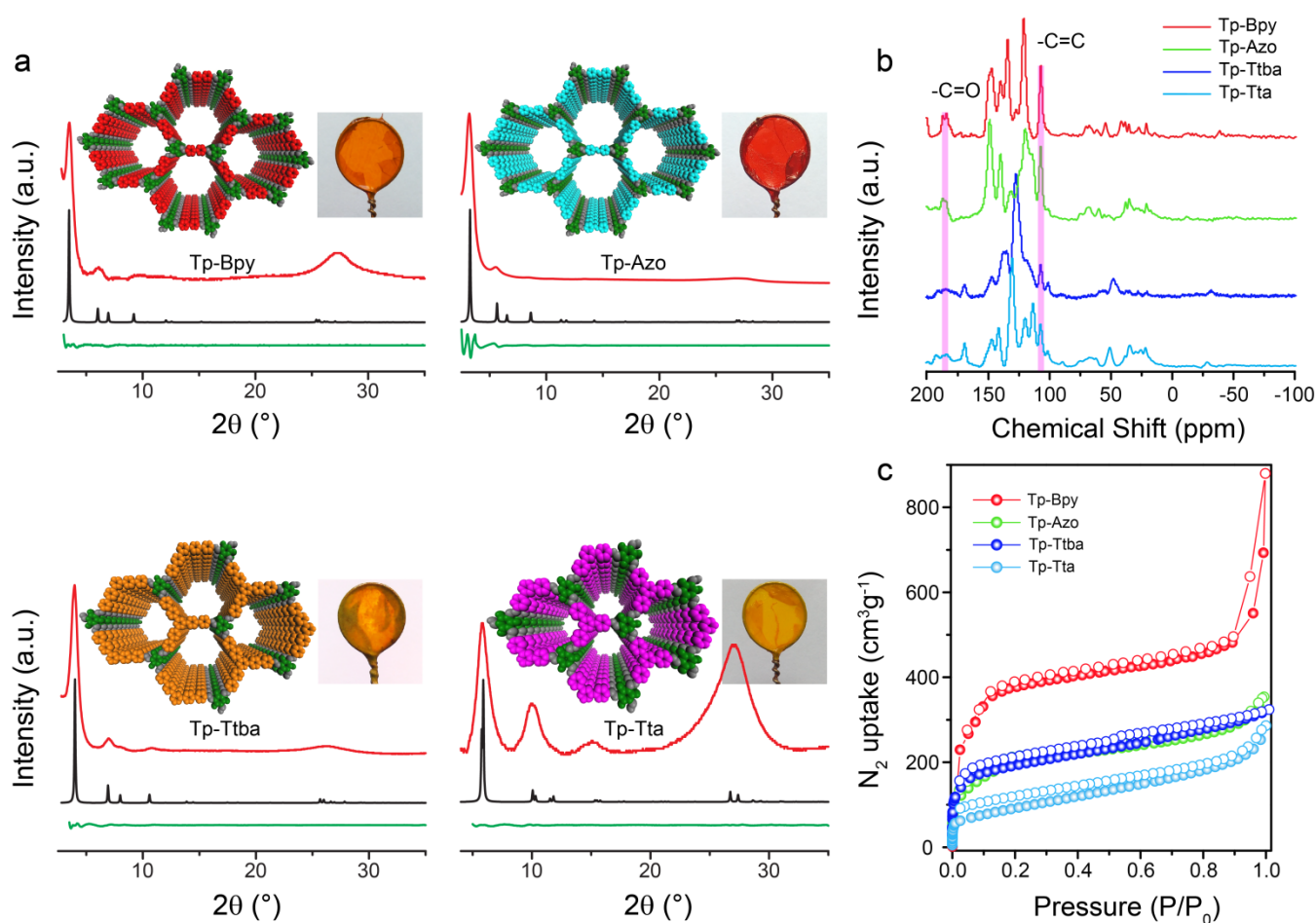


Figure 2. Structural characterization of thin films. (a) Comparison of the experimental PXRD patterns (red) of COF thin films with the simulated eclipsed stacking model (black) and their Pawley refinement difference (green). Space filled models for each of the thin films are shown for AA stacking mode. Inset images show freestanding thin films transferred to a wire loop. (b), (c) Comparison of ^{13}C CP-MAS and N_2 adsorption isotherms of all four COF thin films presented in this work, respectively.

triazine-2,4,6-triyl) trianiline (Tta), 26.5 mg]-PTSA (0.225 mmol, 38.7 mg) were dissolved in 100 mL of water [70 mL water and 30 mL acetonitrile in case of triamines] and added slowly on top of the spacer solution over a period of 30 min. The system was kept at room-temperature for 72 h in undisturbed condition. The thin films formed at the interface were collected by removing the top aqueous layer with a dropper, and washed with water, DMAc and acetone to purify the COFs. The yields of the COFs are **Tp-Bpy** (23 %), **Tp-Azo** (46 %), **Tp-Ttba** (37 %) and **Tp-Tta** (15 %).

PXRD analysis: Powder X-ray diffraction (PXRD) patterns were recorded on a Rigaku, Micromax-007HF with a high-intensity Microfocus rotating anode X-ray generator. All the COF thin films were pasted on an aluminium holder and the data was collected using a Rigaku, R axis IV ++ detector using $\text{Cu K}\alpha$ (1.54 Å) radiation.

AFM analysis: Atomic force microscope (Agilent Technologies, USA, Model 5100) was used to characterize the morphology of the surface of the COF films. Small scanner head was used with a scanning range of $9\ \mu\text{m} \times 9\ \mu\text{m}$ and Z range of $8\ \mu\text{m}$. The samples were scanned in Intermittent Contact Mode or Tapping Mode with a Silicon Cantilever (PPP-NCL, Nanosensors, Inc., USA) having a resonating frequency in the range of 146 – 236 kHz. The nominal diameter of the

silicon tip is $8 \pm 2\ \text{nm}$ and the shape of the tip is four sided. Raster scanning was performed at a speed of 0.50 lines per second with a resolution of 512 points per line.

Fabrication of COF thin-film composites: **Tp-Bpy** and **Tp-Azo** thin films, synthesized in a beaker, were lifted on a polyester-3329 nonwoven porous fabric support and covered with another support from the top. The resulting sandwiched composite was cut into circular coupons of 1 cm diameter and used for the separation experiments.

Solvent flux measurements: All solvent permeations were performed with 1 cm coupons fitted on a dead-end mode stirred cell ($2.54\ \text{cm}^2$ active area) at 1 bar (also 0.5 and 1.5 bar for pressure dependent permeation) upstream pressure. Solvent flux values reported are the average of triplicate experiments conducted with 3 different coupons. Solvent flux (J) was determined by measuring permeate volume (V) per unit area (A) per unit time (t) according to the equation:

$$J = \frac{V}{A \cdot t} \text{ in liters per square meter hour (Lm}^{-2}\text{h}^{-1}\text{)}.$$

Permeance (P) was calculated according to the equation:

$$P = \frac{V}{A \cdot t \cdot \Delta p} \text{ in liters per square meter hour bar (Lm}^{-2}\text{h}^{-1}\text{bar}^{-1}\text{)}.$$

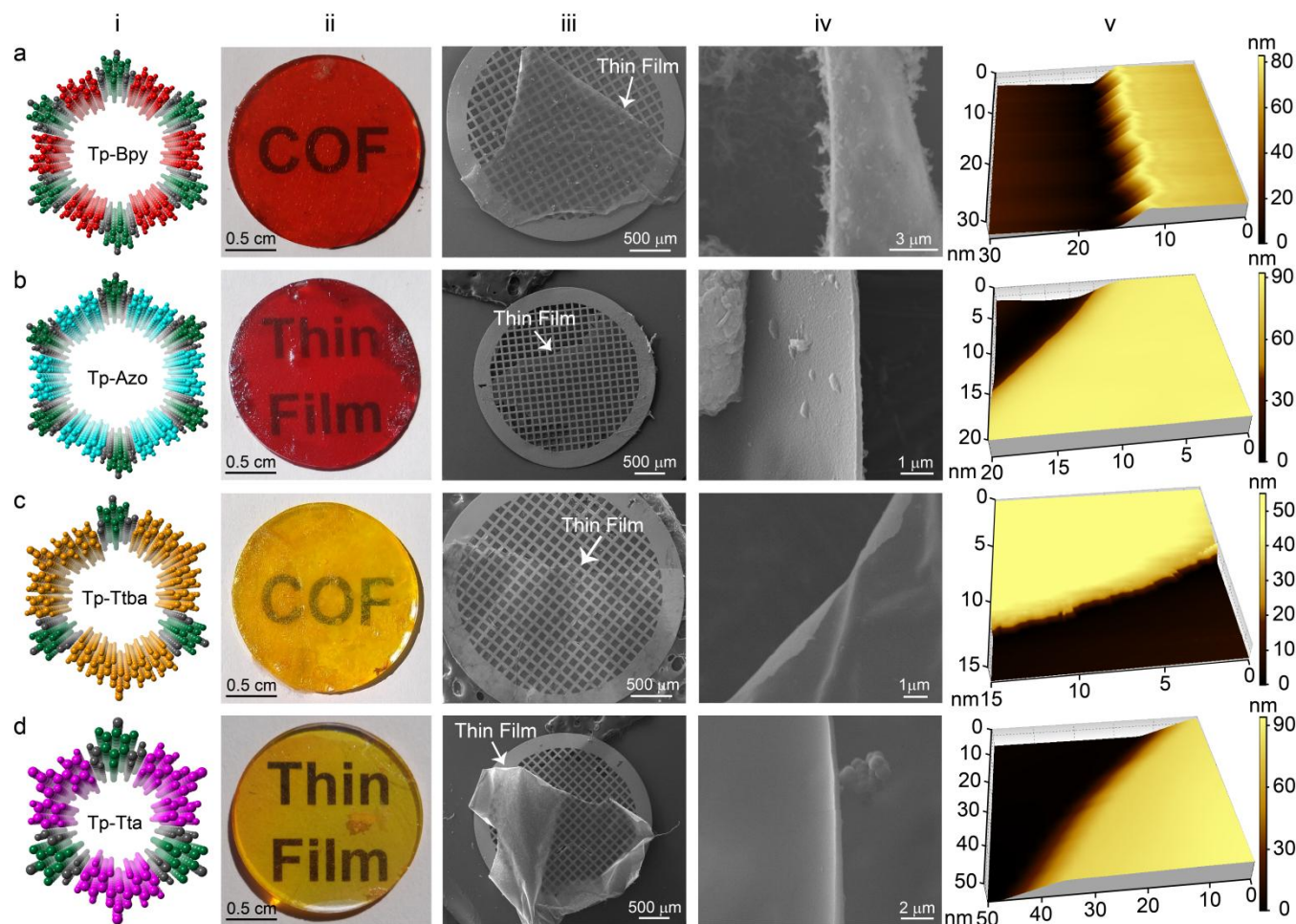


Figure 3. Characterization of transparent thin-films. Synthesized COF thin films: (a) **Tp-Bpy**, (b) **Tp-Azo**, (c) **Tp-Ttba**, (d) **Tp-Tta**. Digital images (ii); SEM (on TEM grid) (iii); SEM (vertical) (iv) and AFM images (v) are shown for the fabricated transparent thin films.

Rejection analysis: Dye rejection was performed by passing 50 μM solutions of dyes through the coupons at 1 bar pressure. Initial 1 ml of the filtrate was discarded and 5 ml was collected for the rejection analysis. Dyes concentration in feed and permeate was determined by a double beam UV-Vis spectrometer (Chemito, Spectrascan UV 2700).

RESULTS AND DISCUSSION

We have adopted the interfacial crystallization technique to synthesize stable keto-enol tautomerism-based^{lh} COF thin films by the Schiff base reaction. As schematically depicted in Fig. 1, three layers of solvents were employed for the synthesis of the COF thin-films. Typically, for synthesizing **Tp-Bpy** thin-films, Tp (0.075 mmol) dissolved in dichloromethane as a bottom layer, the middle layer containing pure water and the topmost layer comprised of Bpy (0.112 mmol)–PTSA (0.224 mmol) salt in water were employed. As dichloromethane and water are immiscible with each other, a liquid-liquid interface is created at the junction of these two solvents. The reaction takes place at room temperature under static conditions over a period of 72 hours in such a way that slow diffusion of alde-

hyde and Bpy-PTSA solution at the interface leads to the crystallization of the **Tp-Bpy** thin film. Here, the presence of the intermediate water layer is highly important as it prevents premature mixing of the precursors and allows slow diffusion, leading to better crystallinity. Controlled experiments without PTSA lead to the formation of amorphous polymer films, which points out the crucial role of PTSA in this interfacial crystallization process (Fig. S18, S19, ESI). Furthermore, in order to check the versatility and general applicability of this method, we have synthesized three more COF thin films of different pore sizes (**Tp-Azo**, **Tp-Tta** and **Tp-Ttba**) using similar concentration of Tp and Azo (0.112 mmol) or Tta (0.075 mmol) or Ttba (0.075 mmol), respectively.

The powder X-ray diffraction (PXRD) was used to ascertain the ordered structure of the as synthesized thin films. Unlike other polymeric thin films, these COF thin films exhibit PXRD patterns, confirming their highly crystalline nature (Fig. 2a). The unique diffraction peaks of the films with respect to the starting building blocks indicate the purity of the thin films obtained at the interface (Fig. S6, ESI). The thin films show intense peaks at lower 2θ values **Tp-Bpy** (3.5°),

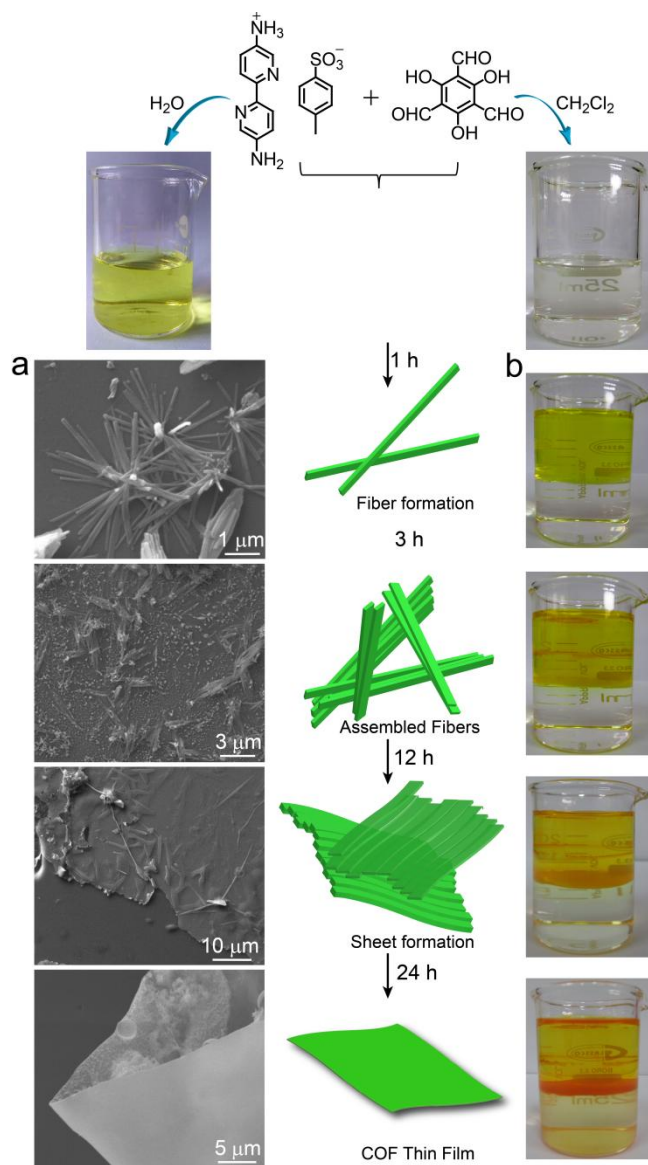


Figure 4. Proposed mechanism for the COF thin film formation (**Tp-Bpy**). (a), (b) SEM and digital images of materials obtained at different stages (fiber formation, assembled fibers and sheet formation) of thin film formation, respectively.

Tp-Azo (3.2°), **Tp-Ttba** (3.9°), which corresponds to the reflections from the 100 plane (Fig. 2a). However, in the case of **Tp-Tta** thin films, the same 100 peak gets shifted to a higher 2θ value of 5.8° due to smaller pore aperture. The broad peak at higher 2θ values (~ 26 – 27°) arises due to the 001 plane reflection (Fig. 2a). The last peak indicates the π - π stacking between successive layers of the thin films. Smaller relative intensity of the first peak with respect to the last peak in case of the **Tp-Tta** thin film denotes less crystalline nature of the film compared to the other three COF thin films. To gain more insight into the structure of these thin films eclipsed and staggered stacking models were constructed in Material Studio-6 (Fig. S4, S7, ESI). Further, we performed Pawley refinement using Reflex Plus module of the Material Studio, which showcases good agreement [**Tp-Bpy** ($R_p = 8.2\%$, $R_{wp} = 7.7\%$); **Tp-Azo** ($R_p = 2.1\%$, $R_{wp} = 3.0\%$); **Tp-Ttba** ($R_p = 12.5\%$, $R_{wp} = 5.9\%$) and **Tp-Tta** ($R_p = 6.2\%$, $R_{wp} = 4.6\%$)] of the

experimental diffraction patterns with simulated AA eclipsed stacking models (Fig. S5, ESI).

The FT-IR spectra of the synthesized thin-films clearly indicate the formation of the β -ketoenamine framework structure. All the thin films show characteristic stretching bands at 1604 – 1623 cm^{-1} ($-\text{C}=\text{O}$); 1565 – 1576 cm^{-1} ($-\text{C}=\text{C}$) and 1267 – 1292 cm^{-1} ($-\text{C}-\text{N}$), matching well with the solvothermally synthesized COF powders (Fig. S9, ESI).^{5a,14} Moreover, the absence of N-H and aldehyde $-\text{C}=\text{O}$ stretching bands at 3100 – 3300 cm^{-1} and 1639 cm^{-1} , respectively, indicates the absence of the starting precursors in the formed films (Fig. S8, ESI). The compositions were further confirmed by ^{13}C CP-MAS solid state NMR spectra, which exhibit characteristic peaks of carbonyl carbons ($-\text{C}=\text{O}$) at ~ 183 – 187 ppm and exocyclic carbons ($-\text{C}=\text{C}$) at $\sim 107\text{ ppm}$. **Tp-Ttba** and **Tp-Tta** thin-films show signals at $\sim 169\text{ ppm}$ for carbons of the triazine ring system (Fig. 2b).

Permanent and tunable porous nature of COFs makes them an ideal candidate for highly permeable membrane applications. Therefore, incorporating this property in COF thin films is of high essence. To access the porosity, we have performed N_2 adsorption analyses of the COF thin films at 77 K . The Brunauer-Emmett-Teller (BET) surface areas calculated for the four thin-films are $1,151$ (**Tp-Bpy**), 647 (**Tp-Azo**), 626 (**Tp-Ttba**) and $333\text{ m}^2\text{g}^{-1}$ (**Tp-Tta**), with total pore volumes of 0.918 , 0.491 , 0.447 and $0.365\text{ cm}^3\text{g}^{-1}$, respectively (Fig. 2c). These surface areas are among the highest for such two-dimensional thin films¹⁵ and nanosheets¹⁶ reported in the literature. NLDFT calculations using equilibrium model reveal narrow size distributions having pore diameters of 2.5 , 2.6 , 1.9 and 1.4 nm for **Tp-Bpy**, **Tp-Azo**, **Tp-Ttba** and **Tp-Tta** thin films, respectively (Fig. S11, ESI). Thermogravimetric analysis (TGA) profiles reveal framework stabilities up to 400°C for the thin films, comparable to the thermal stability of the solvothermally synthesized bulk crystalline powders (Fig. S10, ESI).^{5a,14}

One of the advantages of this interfacial crystallization is the possibility of tuning the thickness of the resulting thin films by just varying the precursor concentrations. Thus, we have fabricated transparent thin films between ~ 50 – 90 nm thickness using a lower precursor concentration [**Tp** (0.018 mmol); **Bpy** (0.028 mmol); **Azo** (0.028 mmol); **Ttba** (0.018 mmol) and **Tta** (0.018 mmol)] as well as thick films having few micrometer dimensions using higher precursor concentrations [**Tp** (0.150 mmol); **Bpy** (0.224 mmol); **Azo** (0.224 mmol); **Ttba** (0.150 mmol) and **Tta** (0.150 mmol)]. To gain insight into the internal structure of the films, we exploited different microscopy imaging techniques such as scanning electron microscopy (SEM), transmission electron microscopy (TEM), atomic force microscopy (AFM), digital optical microscopy, etc. The SEM images revealed a sheet-like morphology of individual layers (lateral dimension more than $100\text{ }\mu\text{m}$) verifying the formation of the thin films (Fig. 1b). Cross-sectional SEM images of the edge of the films revealed uniform thickness [**Tp-Bpy** ($\sim 160 \pm 10\text{ nm}$); **Tp-Azo** ($\sim 150 \pm 10\text{ nm}$); **Tp-Ttba** ($\sim 130 \pm 10\text{ nm}$); **Tp-Tta** ($\sim 190 \pm 10\text{ nm}$)] throughout the sample (Fig. S13, ESI). Transparent thin films were transferred onto silicon wafers and loaded on carbon coated copper TEM grids, before being subjected to SEM imaging. Thin sheet-like morphology is observed with very high lateral dimensions spanning the entire TEM grid having 3 mm diameter (as evident from the horizontal SEM images) (Fig. 3iii). These transparent films were ultrasonicated from a

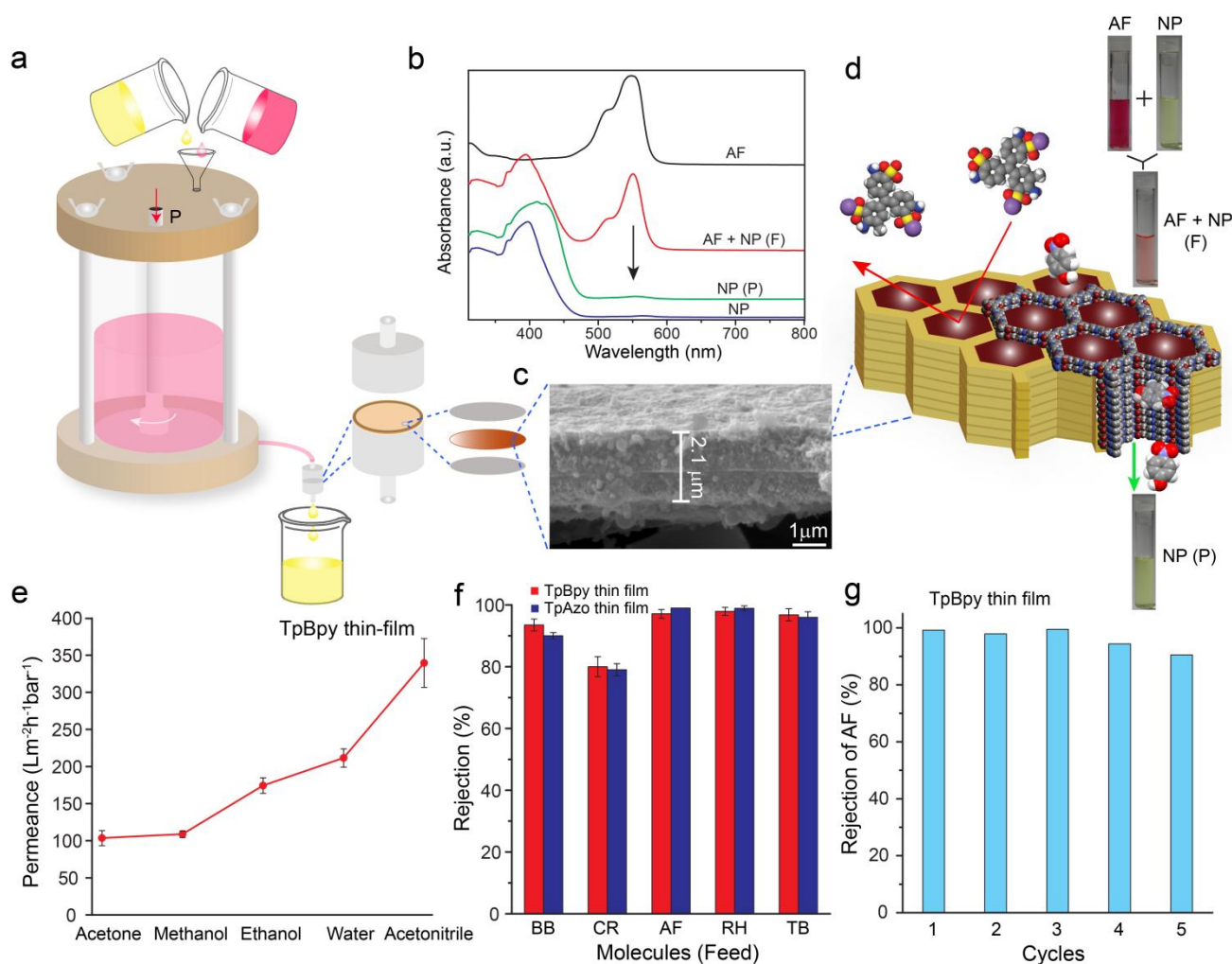


Figure 5. Application of COF thin films in nanofiltration. (a) Schematic illustration of the nanofiltration assembly showing selective molecular separation of *p*-nitrophenol (NP) from a mixture of NP and acid fuchsin (AF). (b) UV-Vis spectra of AF, AF + NP (F), NP (P), and NP. (c) Cross-section SEM of **Tp-Bpy** thin film. (d) Schematic representation of the selective separation through ordered pore structure of **Tp-Bpy** thin film. (e) Pure solvent permeances for **Tp-Bpy** thin film. (f) Nanofiltration performance of **Tp-Bpy** and **Tp-Azo** thin films using different molecules [brilliant blue-G (BB), congo red (CR), acid fuchsin (AF), rhodamine B (RH) and thymolphthalein blue (TB)]. (g) Recyclability of the **Tp-Bpy** thin film for AF rejection over 24 h for 5 cycles.

dispersed solution of isopropanol and dropcasted on silicon wafers for AFM imaging. Height analysis from the silicon wafer to the film surface revealed the thickness of the films in sub-100 nm domain. Thicknesses of these transparent films obtained are ~75 nm (**Tp-Bpy**), ~90 nm (**Tp-Azo**), ~45 nm (**Tp-Ttba**) and ~90 nm (**Tp-Tta**) corresponding to a very high aspect ratio (Fig. S15, ESI). Further close inspection from AFM analysis also discloses rough surface of the thin films comprised of ribbon like COF crystallites (Fig. S21c, ESI).

These self-standing thin films were transferred to various substrates as well as mounted on a 'U' shaped glass loop, where we have observed stable and defect free morphologies for several weeks confirming their mechanical robustness (Fig. S16, ESI). To evaluate their chemical stability, each of the thin films were suspended in water, 3N HCl, *N,N'*-dimethylacetamide and acetonitrile for three days. All the films retained their physical appearance even after such harsh treatments. PXRD analyses of these treated films confirm the retention of the crystallinity and structural integrity (Fig. S17,

ESI). The chemical stability stems from the keto-enamine backbone structure, making them suitable for solvent nanofiltration applications.^{11d,17b}

Mechanism: To shed more light on the crystallization process of the COF thin films, we have executed time dependent electron microscopy studies during **Tp-Bpy** thin film formation (Fig. 4). SEM images of the solution drop cast from the interface after 1 h of addition of amine solution into aldehyde solution revealed a fibrillar morphology having 50-100 nm width and 0.5-1 μm length of the crystallites. As time progresses, these fibers connect laterally to grow into two-dimensions, as seen in the SEM images of the same sample after 3 h of addition. After 12 h of addition, a thin layer appears at the interface, which shows sheet-like morphology along with the presence of fibers. At 24 h, the thin layer becomes more prominent with the disappearance of the fibers. The final form of the same thin film after 72 h illustrates sheet-like layers comprising the two-dimensional architecture. TEM images of the sonicated thin films show extended fibers

with entwined strands forming cobweb-like features (Fig. S14, ESI). Thus, we anticipate self-assembly of the fiber-like crystallites to form a large thin layer of COFs connected entirely by covalent bonds (Fig. S21, ESI). To investigate more about the crystallization process, we performed time dependent FT-IR and PXRD analysis (Fig. S20, ESI). We observed that with the progress of the time, the characteristic peaks of starting precursor aldehyde (Tp) and amine (Bpy) start to disappear and new peaks corresponding to the new bond formation start to appear. For example, -C=O of Tp at 1639 cm^{-1} starts to disappear and -C=O of the COF starts to appear at 1604 cm^{-1} , which becomes prominent at 36 h after the addition. Similarly, characteristic stretching frequencies of the β -ketoenamine backbone structure at 1569 cm^{-1} (-C=C) and 1262 cm^{-1} (-C-N) start to appear at 36 h. A similar closer inspection through PXRD analysis revealed that crystallinity originates and subsequently starts enhancing as the time progresses (Fig. S20b, ESI). We observed the appearance of the first peak at 2θ value of 3.5° after 24 h of addition. This is consistent with the morphology study since initial fiber forms disappear at 24 h and film formation is observed.

PTSA has acted as a 'solid acid catalyst' for the Schiff base reaction, and also as a modulator during the COF synthesis.^{14c} However, unlike solid state synthesis where the role of PTSA is more like a water reservoir, interfacial crystallization occurring at liquid phase demands a slightly different function of PTSA. Protonation of the amine functionality decreases the effective concentration of amine in the solution and regulates the reaction at the interface. It is noteworthy that interfacial crystallization takes place at room temperature under dilute conditions. So, the thermodynamics of the reaction is governed by the slow approach of the aldehyde and amine from opposite directions of the interface. We surmise that nucleation starts when the Schiff base reaction produces low molecular weight monomers and oligomers having fibrous networks, which further polymerize *via* covalent bond formation to grow in two-dimensions but does not show any diffraction pattern. After 24 h these laterally grown layers start to stack *via* π - π interaction and show the diffraction peaks. From 24 h to 72 h these sheets grow in the vertical dimension (100 plane), which is revealed by the increasing intensity of the diffraction peak at $3.5^\circ 2\theta$. This leads to the crystallization of the COFs at the interface.

Molecular Separation: It is well established that membrane separation technology is one of the alternatives to the energy consuming classical industrial techniques such as evaporation and distillation.¹⁷ Since fabrication of freestanding COF thin films at the solution interface is realized without any complicated knife-casting or baking at high temperature, we thought to implement these COF thin films for nanofiltration application. **Tp-Bpy** and **Tp-Azo** thin films, which have larger pore apertures, were chosen for the detailed membrane separation study. Since reducing the thickness to nanometer domain severely compromises the mechanical strength, thin films with optimized thickness **Tp-Bpy** ($2.1\ \mu\text{m}$) and **Tp-Azo** ($5.3\ \mu\text{m}$) were integrated in between two macroporous polyester-3329 supports, and evaluated for molecular separation performance (Fig. S22, ESI). We performed the permeation experiments in a dead-end mode stirred cell (500 rpm) at $30\text{ }^\circ\text{C}$ under 1 bar upstream pressure (Fig. S26, ESI).

The permeation properties of these two COF thin films were studied by passing protic and aprotic organic solvents. The

Tp-Bpy thin film exhibits excellent permeance towards both aprotic and protic solvents such as acetonitrile ($339\text{ Lm}^{-2}\text{h}^{-1}\text{bar}^{-1}$), followed by water ($211\text{ Lm}^{-2}\text{h}^{-1}\text{bar}^{-1}$), ethanol ($174\text{ Lm}^{-2}\text{h}^{-1}\text{bar}^{-1}$) and methanol ($108\text{ Lm}^{-2}\text{h}^{-1}\text{bar}^{-1}$). The acetonitrile and water permeance values are higher than polyamide-based nanofiltration membranes reported in the literature (Table T5, ESI).^{11a,11d} The effects of long-term solvent permeation (0-24 h) and applied pressure (0.5-1.5 bar) on both the **Tp-Bpy** and **Tp-Azo** thin films were also evaluated (Fig. S24, S25, ESI). The constancy of methanol permeance for 24 h confirms that the internal structures of the films are highly stable (Fig. S24, ESI). In order to validate the significance of reduced thickness, we have performed water permeation experiments with **Tp-Bpy** thin films having different thickness. Indeed, decreasing the thickness of the COF layer leads to an increase in the flux value (Table T4, ESI).

Large amounts of wastewater, which contain carcinogenic organic residues, mostly come from the textile and dye manufacturing processes.¹⁸ These dye molecules are very difficult to treat because they are not only resistant to aerobic digestion, but also to heat and light. These dye discharges can cause serious health hazards, since most of them are carcinogenic and mutagenic in nature.^{18b} Therefore, to assess the performance of the thin films towards rejection of a series of contaminants with industrial as well as environmental significance, we conducted filtration experiments with different organic dye molecules. Four organic dye molecules: brilliant blue-G (BB), congo red (CR), acid fuchsin (AF) and rhodamine B (RH) were chosen for this purpose. 30 mL of such dye feed aqueous solution was passed through the stirred cell assembly at 0.5 bar upstream pressure and 5 mL of permeate was collected using each of the thin film membranes. Dye concentration of both feed and permeate was measured by using UV-Vis spectroscopy. The percent rejection (% R) was calculated according to the equation:

$$\% R = \left[1 - \left(\frac{C_p}{C_f} \right) \right] \times 100$$

where C_p is the permeate concentration and C_f is the feed concentration. Both these thin films show very high solute rejection performance. **Tp-Bpy** exhibits rejection values as high as 94 % (BB), 80 % (CR), 97 % (AF) and 98 % (RH); whereas those for **Tp-Azo** are 90 % (BB), 79 % (CR), 99 % (AF) and 99 % (RH) (Fig. S27, S28, ESI). Filtration of a pH indicator thymolphthalein blue (TB) having high molecular weight (430.5) also shows rejections as high as 96 % and 98 % with **Tp-Bpy** and **Tp-Azo** thin films, respectively. Recyclability of the **Tp-Bpy** thin film was also evaluated by passing $50\ \mu\text{M}$ of AF aqueous solution over 24 h periods (Fig. 5g, S29, ESI). Almost negligible change in rejection performance over five cycles demonstrates the long-term applicability of the thin films. Furthermore, the **Tp-Bpy** thin film was subjected to a mixed feed of AF [MW: 585.5; $\sim 1.19\text{ nm} \times 1.14\text{ nm}$] and *p*-nitrophenol (NP) [MW: 139.1; $\sim 0.66\text{ nm} \times 0.43\text{ nm}$]. As shown in Fig. 5a, selective rejection of AF from the mixture was observed in the case of **Tp-Bpy** thin films, which was further confirmed by the UV-Vis spectrum (Fig. 5b).

CONCLUSION

In summary, a versatile synthetic methodology has been demonstrated for the fabrication of COF thin-films to overcome the challenges of processability of COF crystallites as thin-films using a liquid-liquid interfacial technique. The inter-

facial crystallization approach enables the direct formation of high aspect ratio COF layers with simultaneous control of their thickness. These nanoporous COF thin films showcase enhanced permeability in broad solvent range as well as excellent selectivity compared to the nanofiltration membranes reported in the literature. We anticipate that the synthesis technique reported herein for the fabrication of defect free freestanding COF thin films would broaden the realm of practical application of these multifunctional materials. Moreover, appropriate linker selection combined with this powerful approach could facilitate future exploration of COF thin film based sensors and of electronic device fabrication.

ASSOCIATED CONTENT

Synthesis, crystallographic and characterization details are provided in Supporting Information file. This material is available free of charge *via* the Internet at <http://pubs.acs.org>.

AUTHOR INFORMATION

Corresponding Author

* r.banerjee@ncl.res.in.

Author Contributions

‡KD and MP have contributed equally.

Notes

The authors declare no competing financial interests.

ACKNOWLEDGMENT

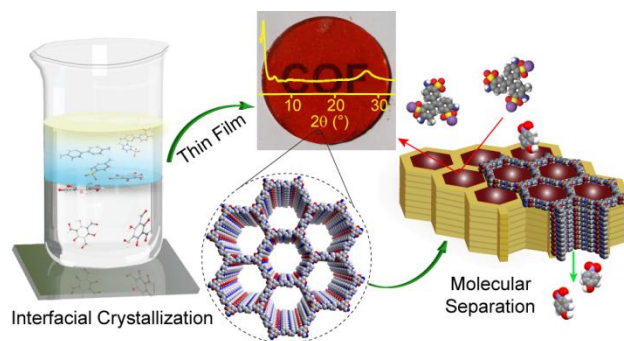
KD acknowledges CSIR, Government of India for Junior Research Fellowship. MP (PDF/2015/000498) and KCR (PDF/2016/000394) acknowledge SERB for a postdoctoral fellowship. RB acknowledges CSIR [CSC0122 and CSC0102], DST (SB/SI/IC-32/2013), DST Indo-Singapore Project (INT/SIN/P-05) and DST Nano-mission Project (SR/NM/NS-1179/2012G) for funding. UKK acknowledges CSIR [CSC0122 and CSC0115]. We acknowledge Dr. T. G. Ajithkumar for providing solid state NMR, and Dr. G. Kumaraswamy for PXRD facility. We acknowledge Dr. P. Pachfule for his valuable comments and suggestions.

REFERENCES

- (1) (a) Côté, A. P.; Benin, A. I.; Ockwig, N. W.; Matzger, A. J.; O’Keeffe, M.; Yaghi, O. M. *Science* **2005**, *310*, 1166. (b) Fang, Q.; Zhuang, Z.; Gu, S.; Kaspar, R. B.; Zheng, J.; Wang, J.; Yan, Y. *Nat. Commun.* **2014**, *5*, 4503. (c) Kuhn, P.; Antonietti, M.; Thomas, A. *Angew. Chem. Int. Ed.* **2008**, *47*, 3450. (d) Wu, Z. S.; Chen, L.; Liu, J. Z.; Parvez, K.; Liang, H. W.; Shu, J.; Sachdev, H.; Graf, R.; Feng, X. L.; Müllen, K. *Adv. Mater.* **2014**, *26*, 1450. (e) Pfeiffermann, M.; Dong, R.; Graf, R.; Zajaczkowski, W.; Gorelik, T.; Pisula, W.; Narita, A.; Müllen, K.; Feng, X. *J. Am. Chem. Soc.* **2015**, *137*, 14525. (f) Dogru, M.; Sonnauer, A.; Gavryushin, A.; Knochel, P.; Bein, T. *Chem. Commun.* **2011**, *47*, 1707. (g) DeBlase, C. R.; Dichtel, W. R. *Macromolecules* **2016**, *49*, 5297. (h) Kandambeth, S.; Mallick, A.; Lukose, B.; Mane, M. V.; Heine, T.; Banerjee, R. *J. Am. Chem. Soc.* **2012**, *134*, 19524. (i) Ma, H.; Ren, H.; Meng, S.; Yan, Z.; Zhao, H.; Sun, F.; Zhu, G. *Chem. Commun.* **2013**, *49*, 9773. (j) Smith, B. J.; Overholts, A. C.; Hwang, N.; Dichtel, W. R. *Chem. Commun.* **2016**, *52*, 3690.
- (2) (a) Biswal, B. P.; Chaudhari, H. D.; Banerjee, R.; Kharul, U. K. *Chem. Eur. J.* **2016**, *22*, 4695. (b) Kandambeth, S.; Biswal, B. P.; Chaudhari, H. D.; Rout, K. C.; Kunjattu, H. S.; Mitra, S.; Karak, S.; Das, A.; Mukherjee, R.; Kharul, U. K.; Banerjee, R. *Adv. Mater.* **2017**, *29*, 1603945.
- (3) (a) Ding, S.-Y.; Gao, J.; Wang, Q.; Zhang, Y.; Song, W.-G.; Su, C.-Y.; Wang, W. *J. Am. Chem. Soc.* **2011**, *133*, 19816. (b) Bhadra, M.; Sasmal, H. S.; Basu, A.; Midya, S. P.; Kandambeth, S.; Pachfule, P.; Balaraman, E.; Banerjee, R. *ACS Appl. Mater. Interfaces* **2017**, *9*, 13785.
- (4) (a) Doonan, C. J.; Tranchemontagne, D. J.; Glover, T. G.; Hunt, J. R.; Yaghi, O. M. *Nat. Chem.* **2010**, *2*, 235. (b) Rabbani, M. G.; Sekizkardes, A. K.; Kahveci, Z.; Reich, T. E.; Ding, R.; El-Kaderi, H. M. *Chem. Eur. J.* **2013**, *19*, 3324.
- (5) (a) Chandra, S.; Kundu, T.; Kandambeth, S.; BabaRao, R.; Marathe, Y.; Kunjir, S. M.; Banerjee, R. *J. Am. Chem. Soc.* **2014**, *136*, 6570. (b) Chandra, S.; Chowdhury, D. R.; Addicoat, M.; Heine, T.; Paul, A.; Banerjee, R. *Chem. Mater.* **2017**, *29*, 2074. (c) DeBlase, C. R.; Silberstein, K. E.; Truong, T.-T.; Aburuña, H. D.; Dichtel, W. R. *J. Am. Chem. Soc.* **2013**, *135*, 16821.
- (6) (a) Rowan, S. J.; Cantrill, S. J.; Cousins, G. R. L.; Sanders, J. K. M.; Stoddart, J. F. *Angew. Chem. Int. Ed.* **2002**, *41*, 898. (b) Jin, Y.; Wang, Q.; Taynton, P.; Zhang, W. *Acc. Chem. Res.* **2014**, *47*, 1575.
- (7) (a) Feng, X.; Ding, X.; Jiang, D. *Chem. Soc. Rev.* **2012**, *41*, 6010. (b) Ding, S.-Y.; Wang, W. *Chem. Soc. Rev.* **2013**, *42*, 548. (c) Waller, P. J.; Gandara, F.; Yaghi, O. M. *Acc. Chem. Res.* **2015**, *48*, 3053.
- (8) (a) Biswal, B. P.; Chandra, S.; Kandambeth, S.; Lukose, B.; Heine, T.; Banerjee, R. *J. Am. Chem. Soc.* **2013**, *135*, 5328. (b) Yang, S.-T.; Kim, J.; Cho, H.-Y.; Kim, S.; Ahn, W.-S. *RSC Adv.* **2012**, *2*, 10179. (c) Dogru, M.; Sonnauer, A.; Zimdars, S.; Döblinger, M.; Knochel, P.; Bein, T. *CrystEngComm* **2013**, *15*, 1500.
- (9) (a) Liu, X.-H.; Guan, C.-Z.; Ding, S.-Y.; Wang, W.; Yan, H.-J.; Wang, D.; Wan, L.-J. *J. Am. Chem. Soc.* **2013**, *135*, 10470. (b) Medina, D. D.; Werner, V.; Auras, F.; Tautz, R.; Dogru, M.; Schuster, J.; Linke, S.; Döblinger, M.; Feldmann, J.; Knochel, P.; Bein, T. *ACS Nano* **2014**, *8*, 4042.
- (10) (a) Medina, D. D.; Petrus, M. L.; Jumabekov, A. N.; Margraf, J. T.; Weinberger, S.; Rotter, J. M.; Clark, T.; Bein, T. *ACS Nano* **2017**, *11*, 2706. (b) Wu, Z.-S.; Tan, Y.-Z.; Zheng, S.; Wang, S.; Parvez, K.; Qin, J.; Shi, X.; Sun, C.; Bao, X.; Feng, X.; Müllen, K. *J. Am. Chem. Soc.* **2017**, *139*, 4506. (c) Cho, S.; Yang, F.; Sun, G.; Eller, M. J.; Clark, C.; Schweikert, E. A.; Thackeray, J. W.; Trefonas, P.; Wooley, K. L. *Macromol. Rapid Commun.* **2014**, *35*, 437. (d) Schaak, R. E.; Mallouk, T. E. *Chem. Mater.* **2000**, *12*, 2513.
- (11) (a) Karan, S.; Jiang, Z.; Livingston, A. G. *Science* **2015**, *348*, 1347. (b) Karan, S.; Samitsu, S.; Peng, X.; Kurashima, K.; Ichinose, I. *Science* **2012**, *335*, 444. (c) Yip, N. Y.; Phillip, W. A.; Schiffman, J. D.; Elimelech, M. *Environ. Sci. Technol.* **2010**, *44*, 3812. (d) Jimenez-Solomon, M. F.; Song, Q.; Jelfs, K. E.; Munoz-Ibanez, M.; Livingston, A. G. *Nat. Mater.* **2016**, *15*, 760. (e) Vandezande, P.; Geversb, L. E. M.; Vankelecom, I. F. J. *Chem. Soc. Rev.* **2008**, *37*, 365.
- (12) (a) Matsuoka, R.; Sakamoto, R.; Hoshiko, K.; Sasaki, S.; Masunaga, H.; Nagashio, K.; Nishihara, H. *J. Am. Chem. Soc.* **2017**, *139*, 3145. (b) Sahabudeen, H.; Qi, H.; Glatz, B. A.; Tranca, D.; Dong, R.; Hou, Y.; Zhang, T.; Kuttner, C.; Lehnert, T.; Seifert, G.; Kaiser, U.; Fery, A.; Zheng, Z.; Feng, X. *Nat. Commun.* **2016**, *7*, 13461. (c) Dai, W.; Shao, F.; Szczerbiński, J.; McCaffrey, R.; Zenobi, R.; Jin, Y.; Schlüter, A. D.; Zhang, W. *Angew. Chem. Int. Ed.* **2016**, *55*, 213. (d) Ameloot, R.; Vermoor-tele, F.; Vanhove, W.; Roefiaers, M. B. J.; Sels, B. F.; Vos, D. E. *D. Nat. Chem.* **2011**, *3*, 382.
- (13) El-Kaderi, H. M.; Hunt, J. R.; Mendoza-Cortés, J. L.; Côté, A. P.; Taylor, R. E.; O’Keeffe, M.; Yaghi, O. M. *Science* **2007**, *316*, 268.
- (14) (a) Shinde, D. B.; Aiyappa, H. B.; Bhadra, M.; Biswal, B. P.; Wadge, P.; Kandambeth, S.; Garai, B.; Kundu, T.; Kurungot, S.; Banerjee, R. *J. Mater. Chem. A* **2016**, *4*, 2682. (b) Gomes, R.; Bhaumik, A. *RSC Adv.* **2016**, *6*, 28047. (c) Karak, S.;

- 1 Kandambeth, S.; Biswal, B. P.; Sasmal, H. S.; Kumar, S.;
2 Pachfule, P.; Banerjee, R. *J. Am. Chem. Soc.* **2017**, *139*, 1856.
- 3 (15) (a) Bisbey, R. P.; DeBlase, C. R.; Smith, B. J.; Dichtel, W. R. *J.*
4 *Am. Chem. Soc.* **2016**, *138*, 11433. (b) Rodenas, T.; Luz, I.;
5 Prieto, G.; Seoane, B.; Miro, H.; Corma, A.; Kapteijn, F.;
6 Llabrés i Xamena, F. X.; Gascon, J. *Nat. Mater.* **2015**, *14*, 48. (c)
7 Smith, B. J.; Parent, L. R.; Overholts, A. C.; Beaucage, P. A.;
8 Bisbey, R. P.; Chavez, A. D.; Hwang, N.; Park, C.; Evans, A.
9 M.; Gianneschi, N. C.; Dichtel, W. R. *ACS Cent. Sci.* **2017**, *3*,
10 58.
- 11 (16) (a) Nair, R. R.; Wu, H. A.; Jayaram, P. N.; Grigorieva, I. V.;
12 Geim, A. K. *Science* **2012**, *335*, 442. (b) Mitra, S.; Sasmal, H.
13 S.; Kundu, T.; Kandambeth, S.; Illath, K.; Díaz, D. D.; Banerjee,
14 R. *J. Am. Chem. Soc.* **2017**, *139*, 4513.
- 15 (17) (a) Lively, R. P.; Sholl, D. S. *Nat. Mater.* **2017**, *16*, 276. (b)
16 Marchetti, P.; Jimenez Solomon, M. F.; Szekeley, G.; Livingston,
17 A. G. *Chem. Rev.* **2014**, *114*, 10735.
- 18 (18) (a) Robinson, T.; McMullan, G.; Marchant, R.; Nigam, P.
19 *Bioresource Technology.* **2001**, *77*, 247. (b) de Lima, R. O. A.;
20 Bazo, A. P.; Salvadori, D. M. F.; Rech, C. M.; Oliveira, D. P.;
21 Umbuzeiro, G. A. *Mutat. Res.* **2007**, *626*, 53.
- 22
23
24
25
26
27
28
29
30
31
32
33
34
35
36
37
38
39
40
41
42
43
44
45
46
47
48
49
50
51
52
53
54
55
56
57
58
59
60

SYNOPSIS TOC



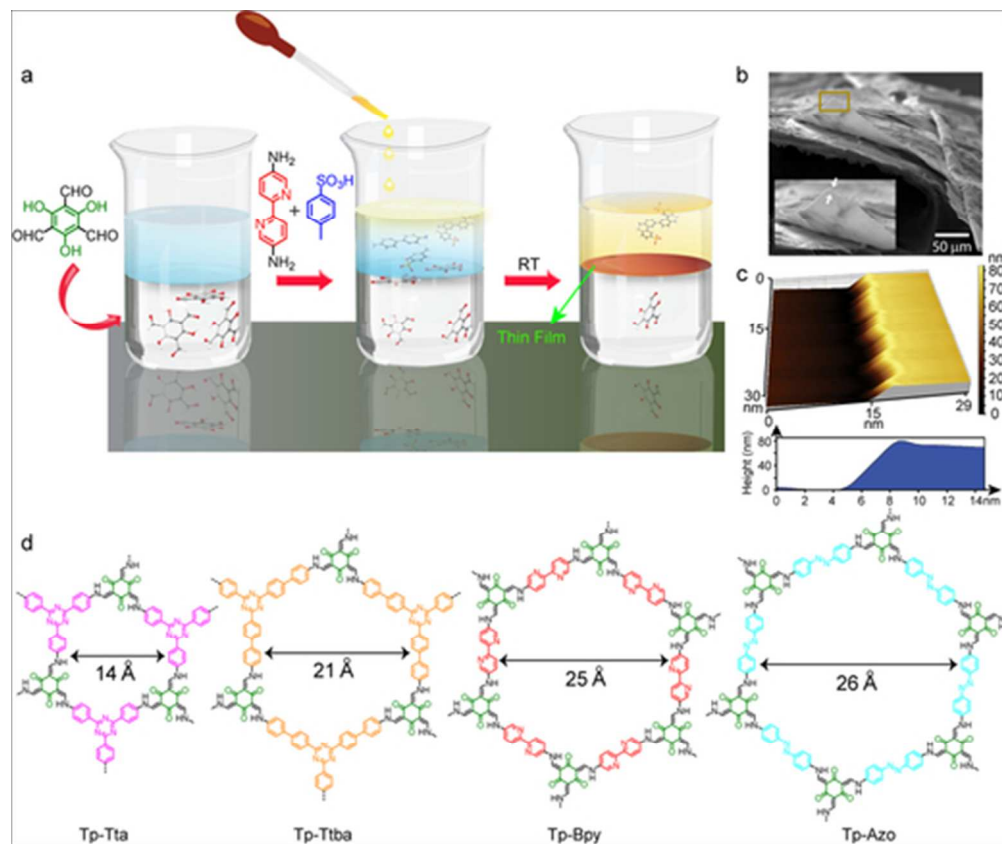


Figure 1

22x18mm (600 x 600 DPI)

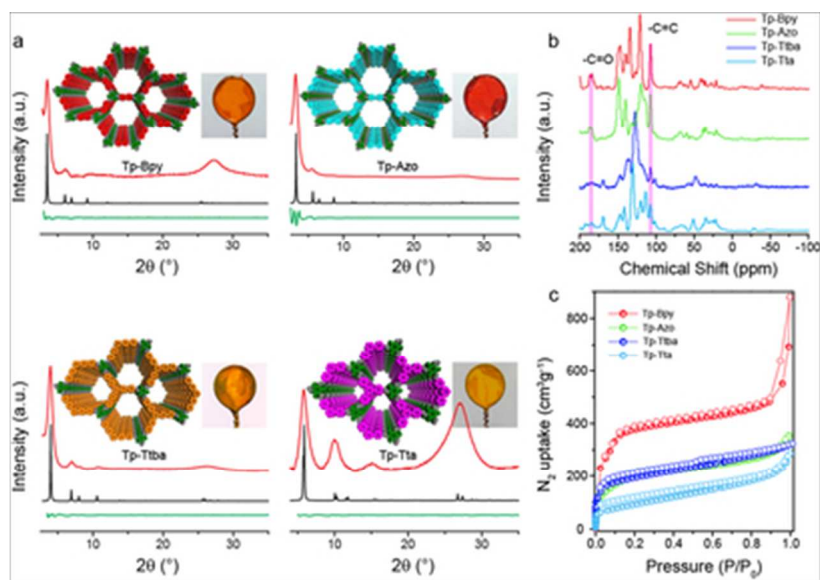


Figure 2

17x12mm (600 x 600 DPI)

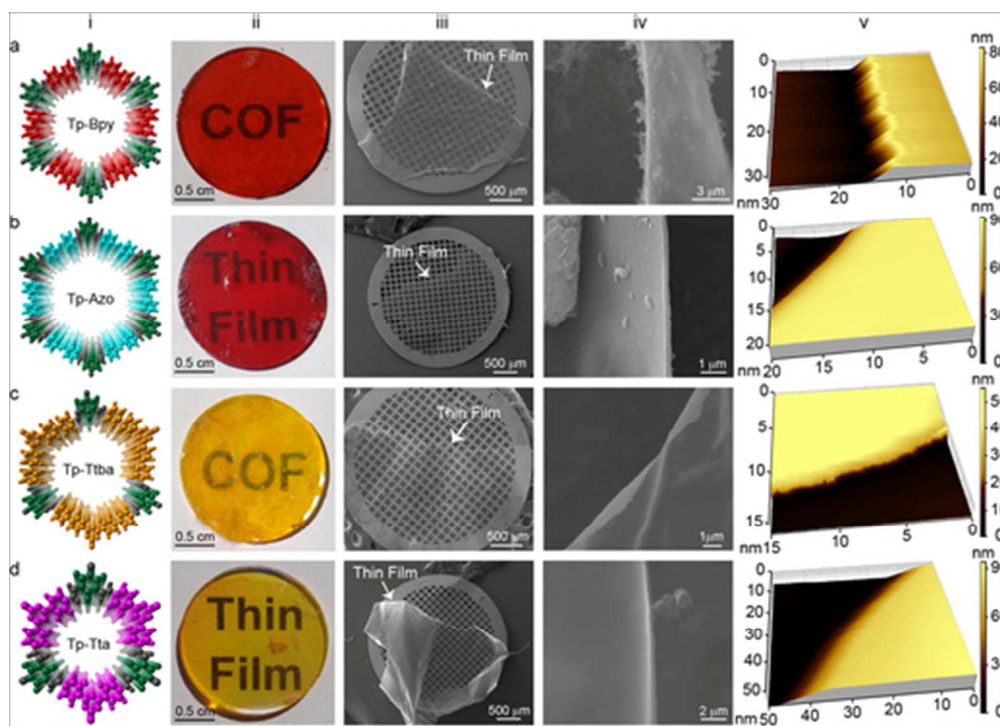


Figure 3

21x15mm (600 x 600 DPI)

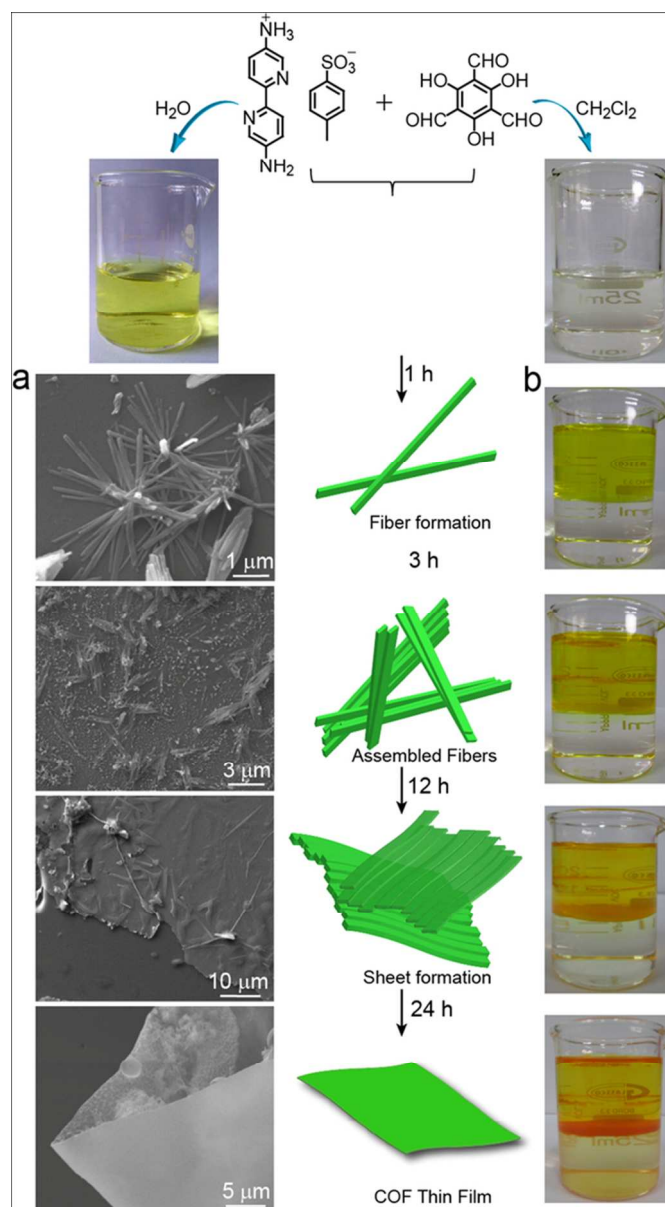


Figure 4

27x50mm (600 x 600 DPI)

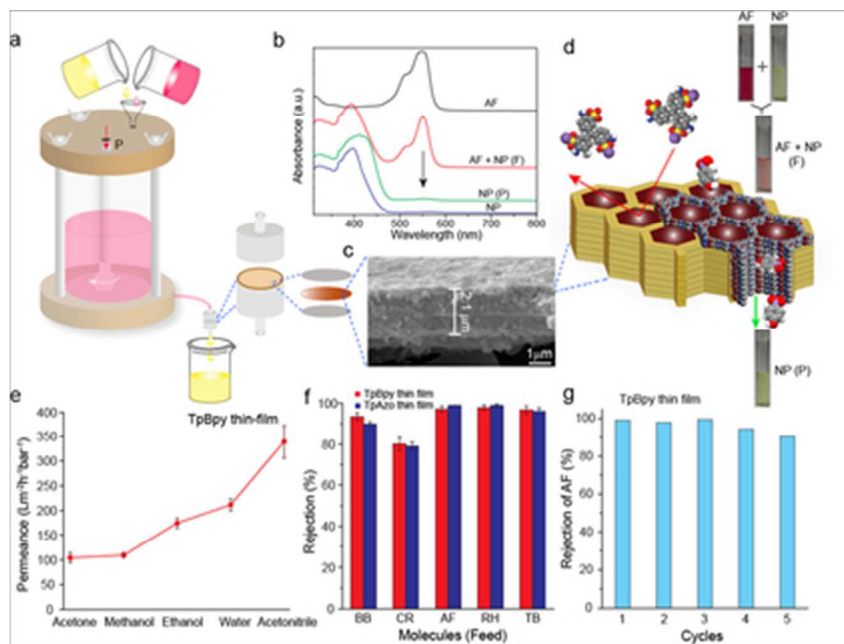
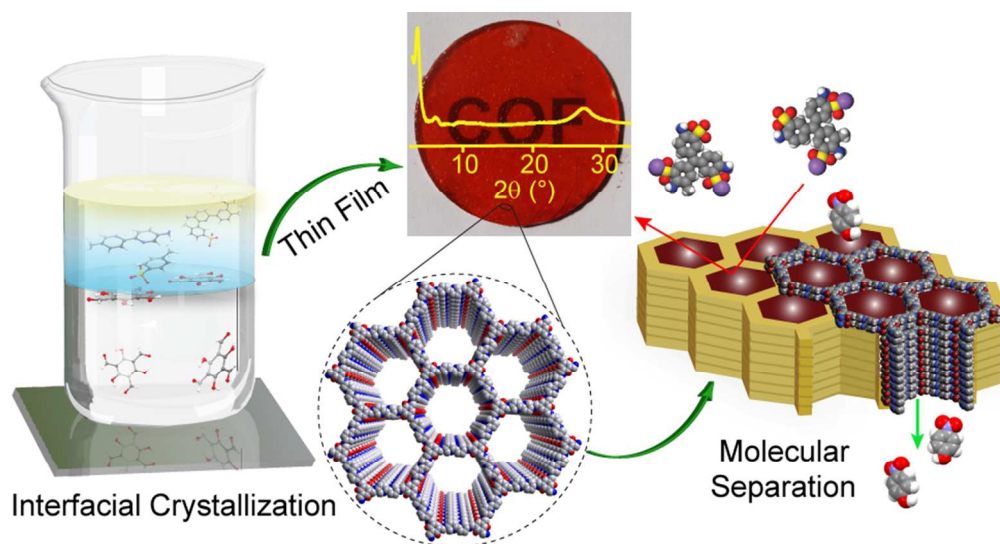


Figure 5

17x13mm (600 x 600 DPI)



TOC-Figure

81x44mm (300 x 300 DPI)